

Galactic Globular Cluster Relative Ages. ¹

A. Rosenberg

Telescopio Nazionale Galileo, Osservatorio Astronomico di Padova, Italy;
rosenberg@pd.astro.it

I. Saviane, G. Piotto

Dipartimento di Astronomia, Università di Padova, Italy;
saviane,piotto@pd.astro.it

A. Aparicio

Instituto de Astrofísica de Canarias, Spain;
aaj@iac.es

Received _____; accepted _____

¹Based on observations collected at the European Southern Observatory, (La Silla, Chile), and the Isaac Newton Group of Telescopes, Observatorio del Roque de los Muchachos, (La Palma, Spain)

ABSTRACT

Based on a new large, homogeneous photometric database of 34 Galactic globular clusters (+ Pal 12), a set of distance and reddening independent relative age indicators has been measured. The observed $\delta(V - I)_{@2.5}$ and $\Delta V_{\text{TO}}^{\text{HB}}$ vs. metallicity relations have been compared to the relations predicted by two recent updated libraries of isochrones. Using these models and two independent methods, we have found that self-consistent relative ages can be estimated for our GGC sample. In turn, this demonstrates that the models are internally self-consistent.

Based on the relative age vs. metallicity distribution, we conclude that: (a) there is no evidence of an age spread for clusters with $[\text{Fe}/\text{H}] < -1.2$, all the clusters of our sample in this range being old and coeval; (b) for the intermediate metallicity group ($-1.2 \leq [\text{Fe}/\text{H}] < -0.9$) there is a clear evidence of age dispersion, with clusters up to $\sim 25\%$ younger than the older members; and (c) the clusters within the metal rich group ($[\text{Fe}/\text{H}] \geq -0.9$) seem to be coeval within the uncertainties (except Pal 12), but younger ($\sim 17\%$) than the bulk of the Galactic globulars. The latter result is totally model dependent.

From the Galactocentric distribution of the GGC ages, we can divide the GGCs in two groups: The old coeval clusters, and the young clusters. The second group can be divided into two subgroups, the “real young clusters” and the “young, but model dependent”, which are within the intermediate and high metallicity groups, respectively. From this distribution, we can present a possible scenario for the Milky Way formation: The GC formation process started at the same zero age throughout the halo, at least out to ~ 20 kpc from the Galactic center. According to the present stellar evolution models, the metal-rich globulars are formed at a later time ($\sim 17\%$ lower age). And finally,

significantly younger halo GGCs are found at any $R_{GC} > 8kpc$. For these, a possible scenario associated with mergers of dwarf galaxies to the Milky Way is suggested.

Subject headings: Hertzsprung-Russell (HR) Diagram – Stars:

Population II – Globular Clusters: General – The Galaxy: Evolution

– The Galaxy: Formation.

1. Introduction

Galactic globular clusters (GGC) are the oldest components of the Galactic halo for which ages can be obtained. The determination of their relative ages and of any age correlation with metallicities, abundance patterns, positions and kinematics provides clues on the formation timescale of the halo and gives information on the early efficiency of the enrichment processes in the proto-Galactic material. The importance of these problems and the difficulty in answering these questions is at the basis of the huge efforts dedicated to gather the relative ages of GGCs in the last 30 years or so [VandenBerg et al. (1996), Sarajedini et al. (1997), and references therein].

The methods at use for the age determination of GGCs are based on the position of the turnoff (TO) in the color-magnitude diagram (CMD) of their stellar population. We can measure either the absolute magnitude or the de-reddened color of the TO. However, in order to overcome the uncertainties intrinsic to any method to get GGC distances and reddening, it is common to measure either the color or the magnitude (or both) of the TO, relative to some other point in the CMD whose position has a negligible dependence on age.

Observationally, as pointed out by Sarajedini & Demarque (1990) and VandenBerg et al. (1990), the most precise relative age indicator is based on the TO color relative to some fixed point on the red giant branch (RGB). This is usually called the “horizontal method”. Unfortunately, the theoretical RGB temperature is very sensitive to the adopted mixing length parameter, whose dependence on the metallicity is not well established, yet. As a consequence, investigations on relative ages based on the horizontal method might be of difficult interpretation, and need a careful calibration of the relative TO color as a function of the relative age (Buonanno et al. 1998). The other age indicator, the “vertical method”, is based on the TO luminosity relative to the horizontal branch (HB). Though this is usually considered a more robust relative age indicator, it is affected both by the uncertainty of

the dependence of the HB luminosity on metallicity and the empirical difficulties to get the TO, and the HB magnitudes for clusters with only blue HBs. It was also pointed out by Sweigart (1997) and Sandquist et al. (1999), that there is the possibility that at a given $[\text{Fe}/\text{H}]$, there may be a dispersion in the content of helium in the envelope HB stars in different clusters. At a given $[\text{Fe}/\text{H}]$, this would lead to a range in HB magnitude and add some scatter to the vertical method of relative age determination.

It must also be noted that both methods are affected by the still uncertain dependence of the alpha elements and helium content on the metallicity.

Given these problems, it is still an open debate whether most GGCs are almost coeval (Stetson et al. 1996) or whether there was a protracted formation epoch of 5 Gyr (Sarajedini et al. 1997) or so (i.e. for 30-40% of the Galactic halo lifetime).

Indeed, there is a major limitation to the large scale GGC relative age investigations: the photometric inhomogeneity and the inhomogeneity in the analysis of the databases used in the various studies. Many previous studies frequently combine photographic and CCD data, different databases (obtained with different instruments with uncertain calibrations to standard systems and/or based on different sets of standards), or inappropriate color-magnitude diagrams (CMD) were used. This inhomogeneity affects even many recent works, for which results can not yet been considered conclusive (see Stetson et al. 1996 for a discussion).

Recently, two new investigations have brought fresh views in this field. First, an analysis of published CMDs both in the B, V and V, I bands was carried out in Saviane et al. (1997; hereafter SRP97). SRP97 showed that the $(V - I)$ TO-RGB color differences are less sensitive to metallicity than the $(B - V)$ ones (while retaining the same age sensitivity). SRP97 also suggested that a high-precision, large-scale investigation in the V and I bands would have allowed a relative age determination through the horizontal method without

the usual limitation of dividing the clusters into different metallicity groups (VandenBerg et al. 1990). Still, a calibration of the horizontal methods in the V and I bands was needed for a correct interpretation of the data.

Later on, Buonanno et al. (1998) showed that, with an appropriate calibration based on the vertical method, reliable relative ages can indeed be obtained with the horizontal method. The investigation of Buonanno et al. (1998) is based both on original and literature ($B - V$) material.

The results presented here take advantage of the strengths of both investigations. Soon after the SRP97 study, we began the collection of an homogeneous photometric material for a large sample of GGCs, in order to obtain accurate relative ages by using the horizontal method in the $([\text{Fe}/\text{H}], \delta(V - I))$ plane. Our first observational effort, aimed at the inner-intermediate halo clusters, is now complete, and we provide here the first results.

In the next section, the data used for this study are presented. In Sect. 3 we define our age indicators and explain how they have been measured on both the CMDs and theoretical models. Section 4 presents the measures obtained following this procedure and compares them with the predictions of the theoretical models. In Sect. 5 we discuss our results. An analysis of the relative ages versus the metallicity (Sect. 5.1) and Galactocentric distance (Sect. 5.3) is presented. The discussion is also carried out comparing clusters in metallicity subgroups (Sect. 5.2). In Sect. 6 the clues obtained till now are used to gather some information on the Milky Way formation and evolution. A summary is finally given in Sect 7. The potentiality of our data base for testing the theoretical calculations is also discussed in Appendix B.

2. The data

The goal of our observational strategy was to obtain color differences near the TO region with an uncertainty $\leq 0.01\text{mag}$, which allows a $\leq 1\text{Gyr}$ age resolution. As a first step, we used 1-m class telescopes to build a large reference sample including all clusters within $(m - M)_V = 16$. The 91cm ESO/Dutch Telescope (for the southern sky GGCs) and the 1m Isaac Newton Group/Jacobus Kapteyn Telescope (for the northern sky GGCs) were then used to cover 52 of the scheduled 69 clusters. Of the total sample, only 34 were suitable for this study. The remaining objects were excluded due to several reasons: differential reddening, small number of member stars, large background contamination, bad definition of the RGB or HB. One or two overlapping fields were covered for each cluster, avoiding the cluster center, especially when it is crowded. From 2500 to 20000 stars per cluster were measured. The typical CMD extends from the RGB tip to ≥ 3 magnitudes below the TO. The final selected sample is listed in Tab. 1. Cluster names are given in col. 2. The assumed $[\text{Fe}/\text{H}]$, which covers almost the entire GGC metallicity range ($-2.1 \leq [\text{Fe}/\text{H}] \leq -0.7$), is given in col. 3. The $[\text{Fe}/\text{H}]$ values were taken (unless otherwise stated) from Rutledge et al. (1997) (their Tab. 2, column 6). Column 4 lists the Galactocentric distance (from Harris 1996), which extends from 2 to ~ 20 kpc. The following columns report our measures, as discussed in Sect. 4.

In our attempt to be as homogeneous as possible, we have adopted the metallicities listed in Rutledge et al. (1997). Their values were in fact obtained from a large and homogeneous work based on the Ca II triplet, and calibrated both over the Carretta & Gratton (1997) and the Zinn & West (1984) scale.

In this paper we adopt the Carretta & Gratton (1997) values, as their metallicity scale was obtained from high resolution CCD spectra of 24 GGCs (20 of them are in common with our sample), analyzed in a self-consistent way. The main results presented in the

following sections would not change adopting the Zinn and West (1984) scale.

A detailed description of the observation and reduction strategies are given in Rosenberg et al. (1999a,b Papers I & II), where the CMDs for the whole photometric sample are also presented. Here suffice it to say that the data have been calibrated with the same set of standards, and that the absolute zero-point uncertainties of our calibrations are ≤ 0.02 mag for each of the two bands. Moreover, three clusters have been observed with both the southern and northern telescopes, thus providing a consistency check of the calibrations: the zero points are consistent within the calibration errors, and, most important, no color term is found between the two data sets.

Only two well known young clusters, Pal 1 (Rosenberg et al. 1998a) and Pal 12 (Rosenberg et al. 1998b, Paper III), have been observed in the V,I bands deep enough to allow the measurement of their TOs. Since Pal 1 has no HB stars, Pal 12 remains the only cluster that allows an extension of the present work to very young clusters: for this reason, it has been included in our analysis, even if its photometry is not strictly homogeneous (different equipment has been used) with that of the other clusters, though the photometric calibration has been done using the same set of standards (Landolt 1992), and at the same level of accuracy.

Figure 1 is an example of our photometry. The CMDs of 4 clusters, representing diagrams covering the whole range in quality of our data, are shown.

3. Methodology

The key point ahead of the present analysis is the totally homogeneous photometric sample that has been obtained. There are several other improvements with respect to previous investigations. In particular, (a) we have used and analyzed three of the most

recent evolutionary models; (b) the theoretical trends of the photometric parameters have been modeled with third-order polynomials in both the age and metallicity instead of straight lines; and (c) a new and more homogeneous metallicity scale (0.05 dex is the typical internal error on $[\text{Fe}/\text{H}]$), calibrated on a large homogeneous spectroscopic sample, has been used.

We now discuss how the two observational databases were used to define our differential age estimators, and how the theoretical models were parameterized in order to convert our parameters into relative ages.

3.1. Differential age estimators

Recent discussions on the possible choices for the photometric parameters (which always measure the TO position with respect to some other CMD feature with negligible dependence on age) can be found in Stetson et al. (1996), Sarajedini et al. (1997) and Buonanno et al. (1998). Our investigation is based on two “classical” reddening and distance independent parameters: the magnitude difference $\Delta V_{\text{TO}}^{\text{HB}}$ between the HB and the TO (vertical method), and the color difference $\delta(V - I)_{@2.5}$ between the TO and the RGB (horizontal method), where the RGB color is measured 2.5 magnitudes above the TO. These quantities are displayed in Fig. 2 for NGC 1851.

A few other parameters, introduced in previous works, have been measured and tested. Vandenberg et al. (1990) were the first to suggest that the point on the MS 0.05 mag redder than the TO, could be a better vertical reference point than the TO itself. This point has been consequently used for analyzing the magnitude difference relative to the HB level (Buonanno et al. 1998) or as a reference point for measuring the RGB-TO color difference 2.5 mag above it (Vandenberg et al. 1990). We found this point useful for the

very best diagrams (~ 10 in our sample), but it is very difficult or impossible to measure it for $\sim 50\%$ of our clusters. Indeed, we must recall that, from the observational point of view, we had to reach a compromise between the deepness of our photometry and the size of the sample that we could collect with a 1-m class telescope. As a result, while the TO position can be reliably measured for all of our selected clusters, the “0.05” point (which is ~ 1 mag fainter than the TO) generally falls in a MS region where the photometric scatter is larger.

One might also question the $\Delta V = 2.5$ mag choice and whether a brighter point on the RGB could be better. To this respect, we must consider that as we go from the TO up to the brighter part of the RGB, the photometric error becomes smaller, but the RGB dependence on $[\text{Fe}/\text{H}]$ gets larger. At the same time, the RGB is less and less populated, so that it can be defined with a lower accuracy. In any case, we made some tests by measuring the TO-RGB color difference for magnitude offsets ranging from 1.5 to 3.5 mag above the TO. We concluded that the $\delta(V - I)_{@2.5}$ parameter represents the best compromise.

3.2. Measurement procedures

In order to measure the morphological parameters, first the fiducial MS lines were found by taking the median of the color distributions obtained in magnitude boxes containing a fixed number of stars, ranging from 50 to 200 stars. The actual number was a function of the total number of stars observed in the cluster. This method allows to adapt the height of the magnitude box to the number of stars that are found in each branch. It has for example the advantage that the TO region, which has a strong curvature, can be sampled with a small magnitude bin ($0.03 \div 0.04$ mag, typically).

The RGBs were defined by fitting an analytic function to the fiducial points starting from ~ 1 mag in V above the TO. We found that a hyperbolic function gives an excellent fit

to these regions, being able to follow the RGB trend even for the most metal rich clusters, (Saviane et al. 1999). In particular, a function of the form:

$$V = a + b(V - I) + c / [(V - I) - d]$$

was used. A dotted line shows the fit to the NGC 1851 RGB in Fig. 2.

The HB level was found from the actual HB stars distribution for each cluster by comparison with an empirically defined fiducial HB. The latter was defined by starting with a bimodal HB cluster (NGC 1851), and extending the HB to the red and to the blue by using our best metal rich and metal poor clusters, respectively. Once the best fit was found, the value V_{HB} was read at a color which corresponds to $(V - I) = 0.2$ on the fiducial HB.

Finally, the turnoff position was found in a two-step procedure. First, a preliminary location was defined by taking the color and the magnitude of the bluest point on the fiducial MS lines; then the color was fine-tuned by computing a statistics of the color distribution near this point. All fiducial points whose colors are within ± 0.01 mag of this preliminary TO position estimate were used to compute the mean value which was assigned to the TO. This step was iterated 20 times, keeping the color box fixed but changing each time the stars that actually enter into the statistical computation, according to the TO position. Usually, the procedure converges very fast.

The measured values for the 35 GGCs are presented in Tab. 1. The TO magnitudes and colors are given in cols. 5 and 6, while the obtained HB level is given in col. 7.

3.3. Observational errors

In order to estimate the uncertainty in the adopted TO color and magnitude, we built a few hundred synthetic CMDs for each cluster, using the Padova library of isochrones (see Bertelli et al. 1994). These CMDs were done adopting for each cluster the corresponding

metallicity, the photometric errors (as estimated from the star dispersion along the MS and lower SGB), and the total number of stars in the observed CMD. All synthetic models corresponding to a given cluster were computed with the same input parameters, varying only the initial random number generator seed. The procedure used to determine the TO (cf. Sec. 3.2) was repeated for the synthetic diagrams associated with each cluster, and the standard deviation of the results was assumed to be the errors actually affecting the color and magnitude of the TO in the observed CMDs.

The errors on the HB level are more difficult to estimate. As explained before, the HB level was found using an empirically defined fiducial HB. The usually small number of stars in this branch and their non linear distribution with magnitude or color (from totally red horizontal branches to nearly vertical blue HBs), does not allow an easy estimate of the uncertainty associated with the HB magnitude.

The errors have been estimated by allowing the empirically defined fiducial HB to move from the upper to the lower envelope of the HB in each cluster. The uncertainties obtained in this way, turned out to be similar among the clusters with red HBs and the clusters with blue HBs, respectively. Therefore, we decide to use a mean error of ~ 0.05 mag for the red HB objects, and ~ 0.10 mag for the blue ones. Note that these uncertainties must be considered an upper value for the error, as among the stars in the brighter HB envelope there are surely evolved HB stars. Our HB level estimates are always within 0.1 mag of the Harris (1996) compiled values, with the exception of four clusters (NGC 6779, NGC 6681, NGC 6093, and NGC 6254) for which more recent published photometry is found in better agreement with our estimates than with Harris (1996).

The estimated error for the RGB colors is the standard deviation of the distribution of the residuals from the fiducial RGB of the color of the stars located between 1.5 and 3.5 magnitudes above the TO. The final error on $\Delta V_{\text{TO}}^{\text{HB}}$ is obtained as the quadratic sum of the

errors on the TO and HB magnitudes, while the error on $\delta(V - I)_{@2.5}$ considers both the error in color and magnitude of the TO (which affects the position of the reference point on the RGB), and the error on the color of the point 2.5 mag brighter than the TO magnitude.

3.4. The theoretical models

In order to interpret the results of our data samples, the theoretical isochrones computed by Straniero et al. (1997, hereafter SCL97), Cassisi et al. (1998, C98), and Vandenberg et al. (1999, V99) were used. These isochrones are the most recent ones which provide $(V - I)$ colors and use updated physics. It is important to notice that these theoretical models are completely independent: indeed, they are obtained with different prescriptions for the mixing-length parameter, the Y vs. Z relation, the temperature-color transformations and bolometric corrections, etc. The differences among the relative ages resulting from the models can be taken as an indication of the (internal) uncertainties intrinsic to our present knowledge of the stellar structure and evolution. The same morphological parameters already defined for the observational CMDs were measured on the isochrones.

The trends of the theoretical quantities as functions of both age and metallicity were least-square interpolated by means of third-order polynomials, so that the observed parameters can be easily mapped into age and metallicity variations. The details of the fitting relations are reported in Appendix A.

In order to calculate the theoretical values of $\Delta V_{\text{TO}}^{\text{HB}}$, we have to assume a relation for the absolute V magnitude of the HB as a function of the metal content. In particular, here we adopted $M_V(ZAHB) = 0.18 \cdot ([\text{Fe}/\text{H}] + 1.5) + 0.65$, from the recent investigation of Carretta et al. (1999). The implications of this choice will be discussed in the following

sections.

4. Clusters' relative ages

In this section, relative ages are obtained from the observed $\Delta V_{\text{TO}}^{\text{HB}}$ and $\delta(V - I)_{@2.5}$ parameters by comparison with the V99 and SCL97 models. As discussed in the Introduction, from the observational point of view, the horizontal method is a more precise relative age indicator than the vertical one (Sarajedini et al. 1990, Vandenberg et al. 1990), as furtherly demonstrated in Sec. 5. Unfortunately, the dependence of the RGB temperature on the the adopted mixing length parameter (whose dependence on the metallicity is not well established yet), and the uncertain run of the alpha elements enhancement, and helium content, with the metallicity (which affect the vertical method as well) makes the data interpretation not straightforward. A detailed analysis of these effects is beyond the purpose of the present paper. However, we made an internal consistency check for the theoretical models, and selected those for which the relative age trend with the metallicity turned out to be same (within the errors) using both the horizontal and vertical method. While the V99 and SCL97 models satisfy this condition (cf. Figs. 3 and 4) for our sample of GGCs, C98 models do not. Further tests are required to identify the source of this problem, but it could be possibly related to the I bolometric corrections (cf. Appendix B), so the C98 model predictions could still be valid for the V and B bands. In any case, because of this internal inconsistency, from here on we will base our analysis on the V99 and SCL97 models only. The implications of the comparison between the observed data and the C98 models will be presented in Appendix B.

We want to note that the *absolute* ages obtained from the two methods are not the same. The age differences between the vertical and horizontal method are ~ 1.2 and ~ 1.5 Gyrs for the SCL and V99 models, respectively. This discrepancy can be removed by

adopting for the V_{HB} vs. $[\text{Fe}/\text{H}]$ relation an appropriate constant. Far of being a problem for our purpose of measuring relative ages, these discrepancies can be a way to test the models and to fine-tune some still uncertain input parameters. These points will be further discussed in Appendix B.

4.1. Ages from the “vertical” method

The measured $\Delta V_{\text{TO}}^{\text{HB}}$ parameter (and the corresponding error) is listed for each cluster in Tab. 1 (col. 8). These values are plotted versus the cluster metallicity in Fig. 3. The dotted lines are the isochrones from the V99 (top) and the SCL97 (bottom) models. Age is spaced by 1 Gyr steps, with the lowermost line corresponding to 18 Gyrs.

We notice in the figure that the clusters are distributed in a narrow band of ≤ 2 Gyrs width, apart from five clusters at $[\text{Fe}/\text{H}]$ values between -1.1 and -0.8 (namely, NGC 2808, NGC 362, NGC 1261, NGC 1851 and Pal 12). Within the observational errors, the theoretical isochrones and the observed values show similar trends with metallicity for $[\text{Fe}/\text{H}] \leq -0.9$. It must be stated that this result depends on the choice of the trend of the HB luminosity with $[\text{Fe}/\text{H}]$, although the conclusions would be the same if the slope of the V_{HB} vs. $[\text{Fe}/\text{H}]$ relation is changed by no more than $\pm 15\%$ (see also below). There is also a small second order dependence of the relative ages on the zero-point of the relation, but this just changes all the relative ages by a constant factor, while the trend with $[\text{Fe}/\text{H}]$ remains unchanged.

The isochrones were used to tentatively select a sample of coeval clusters: first for each stellar evolution library the theoretical locus that best fits the sample (not including Pal 12) was found, and the relative $\Delta V_{\text{TO}}^{\text{HB}}$ with respect to this locus were computed. We then chose to define as coeval GGCs those clusters whose vertical parameter was within ± 1

standard deviation from the best-fitting isochrone. This interval is marked by thick lines in Fig. 3. Objects lying within this interval for both sets of theoretical models (that we will call fiducial coeval from here on) are marked by open circles in Fig. 3 and will be used later on to test the isochrones in the $\delta(V - I)_{@2.5}$ vs. $[\text{Fe}/\text{H}]$ plane. Interestingly enough, the same set of coeval clusters is selected using both the SCL97 and the V99 isochrones, and using any slope α for the V_{HB} vs. $[\text{Fe}/\text{H}]$ relation in the range $0.17 < \alpha < 0.23$ for the V99 isochrones and $0.15 < \alpha < 0.20$ for the SCL97 isochrones. The best fitting isochrones have ages of 14.3 Gyrs according to the V99 models, and 14.9 Gyrs from the SCL97 ones. As it will be discussed below, the actual dispersion of the fiducial coeval clusters around the mean isochrone, is indeed consistent with a null age dispersion.

We now turn our attention to those clusters that depart from the distribution of the fiducial coevals. It must be noted that the discrepancies are always in the sense of younger ages (smaller $\Delta V_{\text{TO}}^{\text{HB}}$): moreover, for the discrepant clusters at $[\text{Fe}/\text{H}] \leq -0.9$, there are counterparts with similar metallicity within the coeval sample, whereas for the more metal-rich clusters the situation is less clear. Indeed, if we rely on the theoretical models, the three most metal rich clusters would seem younger than 47 Tuc. However, it is well-known that problems arise in modeling the RGB of metal rich stars (e.g. Stetson et al.1996), so it could also be the case that the coeval cluster band actually turns up at the metal rich end more than what is predicted by the adopted models. We will have to come back to this point later on.

For a better comparison of the results from the two methods, we calculated what we call the mean normalized age. First, we derived the best mean age of the “coeval” clusters according to each of the two sets of evolutionary models: viz., 14.3 Gyr for V99, and 14.9 Gyr for SCL97. Then, for each cluster, we calculated the ratios of the actual age for that cluster (as deduced from the model grids in the two panels of Fig. 3, cf. also Appendix A)

relative to the mean age, for the two cases. The mean of these two normalized ages are listed in Col. 3 of Tab. 2. The errors are the age intervals covered by the photometric error bars in the normalized age scale. In addition, Col. 4 of the same Table gives the difference between the absolute mean age of each cluster and the absolute age of the bulk of the GGCs, assuming that the latter is 13.2 Gyrs as in Carretta et al. 1999).

The age dispersions resulting from the vertical method are ± 1.4 Gyr (independently from the adopted model) when using the entire sample (excluding Pal 12); when only the fiducial coeval sample is considered, the age dispersions become ± 0.7 and ± 0.6 Gyr using SCL97 and V99 models, respectively. In terms of percent values, this translates into a 9.2% and 9.8% (all clusters minus Pal 12), and 4.4% and 4.5% (coeval sample) age dispersion. These latter dispersions are fully compatible with the uncertainties in the $\Delta V_{\text{HB}}^{\text{TO}}$ values, strengthening the idea that the clusters selected as coeval must indeed have the same age.

4.2. Ages from the “horizontal” method

The measured $\delta(V - I)_{@2.5}$ parameters are presented in Tab. 1 (col. 9) and plotted versus the cluster metallicity in Fig. 4. The dotted lines in the figure represent the isochrones from V99 (upper panel) and SCL97 (lower panel), in 1 Gyr steps. The lowermost lines are the 18 Gyr and 17 Gyr isochrones, respectively.

Remarkably enough, Fig. 4 resembles Fig. 3: again, most clusters are located in a narrow sequence for $[\text{Fe}/\text{H}] \leq -0.9$, with the exception of the same previously identified five clusters, which result to have a younger age also in this case. Also, the trend with metallicity is conserved, with a similar uprise at the metal-rich end.

For the clusters at $[\text{Fe}/\text{H}] \leq -0.9$ dex, the run of $\delta(V - I)_{@2.5}$ is also reproduced by the isochrones. In this metallicity range, the clusters selected as fiducial coeval by the vertical

method (open circles) still fall within a chronologically narrow band of ≤ 2 Gyr, showing a remarkable consistency between the two methods.

Apparently, the metal richer clusters are younger than the bulk of Galactic globulars. Once more, this result is totally model-dependent, and we must recall again that uncertainties in the color-temperature relations and mixing length calibration, as well as the run of the alpha elements content and helium abundance with metallicity, could affect the relative ages obtained for the most metal rich objects (e.g. Stetson et al. 1996). Therefore, a problem with the theoretical relations cannot be excluded, and NGC 104, NGC 6366, NGC 6352 and NGC 6838 could indeed be coeval with the other clusters. Nevertheless, it must be noted that the same trend is present on ages from the vertical method. Moreover, if we apply a 0.07 mag correction for the HB magnitude of the 4 most metal rich clusters (as suggested by Buonanno et al. 1998), the ages obtained from the vertical method would be shifted towards lower values, making them perfectly consistent with the results from the horizontal method. It is therefore tempting to consider the age trend for the metal rich clusters to be a real possibility (which must be furtherly tested with independent methods), although the precise age offset remains to be established. In any case, if we take the metal rich clusters as a single group, their internal age dispersion is comparable to that of the rest of the fiducial coeval clusters.

As for the vertical method, normalized ages were obtained by means of the difference in the $\delta(V - I)_{@2.5}$ parameter with respect to the best fitting isochrones (13.1 Gyr and 16.4 Gyr for the SCL97 and the V99 models, respectively). The resulting values are listed in Tab. 2 (cols. 5 and 6). In the table, the normalized ages (col. 5) are the mean of the two values obtained using the two models, while the age deviations in Gyr given in col. 6 are computed from col. 5 assuming (as done in the previous section) a mean absolute age of 13.2 Gyr (Carretta et al. 1999) for the mean age of the GGC bulk. The errors are the age

intervals covered by the photometric error bars in the normalized age scale.

Since the $\delta(V - I) \div \delta t$ relation depends on the metallicity in a non-linear way, the width covered by the ± 1 standard deviation limits on the $\delta(V - I)_{@2.5}$ parameter (solid lines on Fig. 4) is not constant. However, we find that it goes from 0.010 to 0.007 mag, for the GGC metallicity range $-2.1 \leq [\text{Fe}/\text{H}] \leq -0.7$. This dispersion is comparable to the experimental mean error for the coeval clusters (0.009 mag; cf. Tab. 1).

Using the SCL97 models, the age dispersions that we have from the horizontal method are $\sigma_t = 1.2$ Gyr for the entire sample (with the exception of Pal 12) and $\sigma_t = 0.6$ Gyr (for the fiducial coeval sample) corresponding to a percent age dispersion of 9.2% and 4.3%. Similarly, from the data in the lower panel of Fig. 4 we have $\sigma_t = 1.4$ Gyr and $\sigma_t = 0.6$ Gyr (10.6% and 4.5%). Although the absolute ages of the clusters obtained from each model differ by ~ 3 Gyr, after the normalization the relative ages are very similar. Moreover, these relative ages are also close to those given by the vertical method (cf. Section 4.1).

As anticipated in the Introduction, Fig. 4 shows a mild metallicity dependence of the $\delta(V - I)$ parameter, smaller than that of the corresponding $\delta(B - V)$ parameter (Buonanno et al 1998). Indeed, as shown by Saviane et al. (1997), and confirmed by Buonanno et al. (1998), the slope of the “isochrone” in the ($[\text{Fe}/\text{H}], \delta(B - V)$) plane is $\simeq 0.04$, while taking the coeval clusters at $[\text{Fe}/\text{H}] < -1$ in Fig. 4 the slope of the isochrone is ~ -0.025 . This means that a typical error of 0.1 dex on the $[\text{Fe}/\text{H}]$ translates in a ~ 0.4 Gyr error on the relative cluster age if measured using the traditional $(B - V)$ color, while it yields an error of 0.25 Gyr if the age is measured with the present method.

Moreover, the self-consistency of the ages predicted by the two methods and the two theoretical models strengthen the conclusions by Saviane et al. (1997) that the $\delta(V - I)$ parameter is much more reliable than the $\delta(B - V)$ as a relative age index. On the contrary, using $\delta(B - V)$ and totally independent data sets, both Saviane et al. (1999) and Buonanno

et al. (1998) show that significant discrepancies still exist between the ages predicted by the vertical and horizontal methods.

As recalled in Sect. 1, the cluster Palomar 12 was included in the present investigation, since it provides an excellent reference point for the age calibration. It was found in Paper III that the age of this cluster is 0.68 ± 0.10 that of both 47 Tuc and M5, as already suggested by Gratton & Ortolani (1988) and Stetson et al. (1988). Here we find that the relative age of Pal 12 with respect to 47 Tuc is 0.68, while it is 0.62 with respect to M5, in agreement with our previous investigation. This result is even more striking if we take into account that our old analysis was based on three other independent models.

5. Discussion: Mean Age Distributions

In this section, the age vs. metallicity and Galactocentric distance trends will be discussed. We will use the normalized ages given in Cols. 3 and 5 of Tab. 2 for the vertical and horizontal methods, respectively (the mean of these two values is given in col. 7). Fig 5 plots these normalized ages vs. metallicity (left panels) and Galactocentric distance (right panels). We arbitrarily divided our GGC sample into four metallicity groups: (a) the very metal poor ($[\text{Fe}/\text{H}] < -1.8$, filled circles), (b) the metal poor ($-1.8 \leq [\text{Fe}/\text{H}] < -1.2$, open triangles), (c) the metal intermediate ($-1.2 \leq [\text{Fe}/\text{H}] < -0.9$, filled squares), and, finally, (d) the metal rich ($[\text{Fe}/\text{H}] \geq -0.9$, open diamonds). Notice that Pal 12 is always represented as an asterisk. The values from the vertical (upper panels) and horizontal (lower panels) methods are plotted separately. Fig 5 shows two important features:

- The first one is that the general trend shown by both methods looks similar (within the errors). A direct comparison of the two methods is provided in Fig. 6, where the difference in the normalized relative ages ($\Delta\text{Age}_{\text{Vert}}^{\text{Hor}}$) is plotted vs. the metallicity.

There is a very small dispersion of $\Delta\text{Age}_{\text{Vert}}^{\text{Hor}}$ around the zero level in each metallicity group. A marginal offset from the zero level for the two extreme metallicity groups is present. This could arise either from discrepancies in the models and/or from the assumed relation for the $V_{\text{(HB)}}$ vs. $[\text{Fe}/\text{H}]$ relation. If we were to act just on the HB level, in order to have the same trend from the two methods, we should use a slope $\Delta M_V(\text{HB})/\Delta[\text{Fe}/\text{H}] = 0.08$ or 0.09 for the SCL97 and V99 models, respectively. These values are not consistent with the current estimates of this slope, so a partial correction of the (theoretical) TO positions should also be considered. At this point, it is very important to remark that the assumptions that must be introduced when using the vertical method are not needed when working with the horizontal one. This method relies on a minimum set of assumptions, thus making the interpretation of the age rankings more straightforward. No parameterization of external quantities (like the HB magnitude) is required.

- The second important point is related to the observational errors. The $\Delta V_{\text{HB}}^{\text{TO}}$ values are affected by uncertainties that are $\sim 1.5 - 2.0$ times larger than those estimated for the $\delta(V - I)_{\text{@}2.5}$ parameter. We already commented on the possibility that our errors on $\Delta V_{\text{HB}}^{\text{TO}}$ could be somehow overestimated (and this is also confirmed by the actual dispersion of the points in Fig. 5). On the other side, though the observational errors on $\delta(V - I)_{\text{@}2.5}$ are surely smaller, we still have to cope with the uncertainty (that we can not estimate) on the theoretical colors when calculating the relative ages with the horizontal method. Still, as the observed trends from both the vertical and horizontal methods are very similar, we prefer to base our further discussion mainly on the results obtained from the horizontal method, where the different trends and effects are more clearly put into evidence. In any case, it must be clearly stated that the discussion would not change using the ages from the vertical method.

5.1. Distribution in Metallicity

In Fig. 5 (left panels) the fiducial normalized ages are plotted vs. the cluster metallicities. Several regions of interest can be discerned in the figure, and as a first step, we discuss here the general trends that can be observed.

The dotted line represents the mean zero relative age level for the coeval clusters: 26 out of 35 clusters are distributed around the mean within an age interval $\Delta_{Age} \leq 10\%$ of the mean. They all have $[Fe/H] < -0.9$. In this region, no age-metallicity relation is visible, when we take into account the errors on the ages. Within the intermediate metallicity group, 4 clusters show definitely younger ages than their equal metallicity counterparts, (namely; NGC 1261, NGC 362, NGC 2808 and NGC 1851). Notice also that no younger clusters are detected for $[Fe/H] < -1.2$.

The 5 clusters with the highest metallicities in our sample, have ages significantly smaller than the mean age distribution. Of these, Pal 12 seems definitely younger than its equal metallicity counterparts. The remaining 4 do not show any significant age dispersion. As already discussed in Sect. 4.2, this effect could be due to some problems in the theoretical models at the metal rich end, but we must note the internal consistency of the two methods. This can give some support to the hypothesis that these 4 clusters might be really $\sim 17\%$ younger (and Pal 12 $\sim 40\%$ younger) than the bulk of GGCs. These 4 objects are NGC 6366, NGC 6352, NGC 6838, and NGC 104. Notice that assuming that these metal rich clusters are indeed younger would have a strong consequence on the Galactic formation scenario, as we will discuss in Section 6.

Taking the mean normalized ages (Tab. 2, col.7) within the formerly defined metallicity groups, we find for the very metal poor group a mean normalized age of 0.98 ± 0.03 , for the metal poor group 1.01 ± 0.03 , for the metal intermediate 0.96 ± 0.12 if the younger clusters are included and 1.00 ± 0.04 if they are not, and for the metal rich 0.78 ± 0.10 if Pal 12 is

included and 0.83 ± 0.03 if it is excluded. As it can be seen, the age dispersion does not vary significantly along the metallicity range if only the coeval clusters are considered. If one includes younger clusters into the computation, then the metal intermediate group shows a larger age dispersion. This is a well-known property of the GGCs (see e.g. VandenBerg et al. 1990).

In conclusion, our data do not reveal an age-metallicity relation in the usual sense of age decreasing (or increasing) with metallicity. What is found is an increase of the age dispersion (due to the presence of a few clusters with younger ages than the bulk of the GGCs) for the metal rich clusters, while the lower metallicity ones ($[\text{Fe}/\text{H}] \leq -1.2$) seem to be all coeval. This is in agreement with the results of Richer et al. (1996), Salaris & Weiss (1998), Buonanno et al. (1998). On the other side, Chaboyer et al. (1996) proposed an age-metallicity relation, of the order $\Delta t_9 / \Delta[\text{Fe}/\text{H}] \simeq -4 \text{ Gyr dex}^{-1}$, which is not present in our data set. What happens for clusters with $[\text{Fe}/\text{H}] \geq -0.9$ is totally model dependent; the models suggest a younger age for these objects than for the more metal poor ones, and no age dispersion.

5.2. Testing young candidates within metallicity groups

Comparisons of relative ages have been often limited in the past to clusters of similar metallicity. This indeed reduces the amount of assumptions to be used, and allows an easier check of the relative positions of the fiducial branches of the GGCs. Some “template” globular pairs or groups have many times been used in this exercise. These special comparisons have been done mainly to establish the efficiency of the halo formation but one could question whether the detection of a single younger cluster can lead to any strong conclusion in favor of some preferred Galactic halo formation model. Aside from this consideration, we want to re-examine here some of the special cases that have drawn much

attention in the recent past.

Our checks are made for metallicity groups. Again, the metallicity scale is that of Carretta & Gratton (1997): note that changing the scale would change the absolute values of $[\text{Fe}/\text{H}]$ but not the membership to the metallicity groups. For each group, we will consider those clusters that are significantly younger than other members of the same group, or those objects which for any reasons have received considerable attention in the recent past.

In order to make the reading of the next discussion easier, we will abbreviate the principal papers in this way: Buonanno et al. 1998 = B98, Chaboyer et al. 1996 = C96, Jonhson & Bolte 1998 = JB98, Richer et al. 1996 = R96, Salaris & Weiss 1998 = SW98, Sarajedini & Demarque 1990 = SD90, Stetson et al. 1996 = S96 and Vandenberg et al. 1990 = V90.

Very low metallicity group ($[\text{Fe}/\text{H}] < -1.8$). For this group we found no evidence of age dispersion. We will comment on previous investigations (cf. B98, C96, SW98, V90 and R96) for 4 globulars (NGC 4590, NGC 5053, NGC 6341 and NGC 7078). B98 and R96 assign a younger age to NGC 4590 NGC 5053 and NGC 6341, and C96 agree that the former two should be younger. On the other side, SW98 and V90 find that the very metal poor clusters are all coeval within the errors. Our Table 2 formally indicate that NGC 4590 and NGC 5053 are slightly younger than the other two; however these differences are smaller than the quoted errors, and therefore not significant.

Low metallicity group ($-1.8 \leq [\text{Fe}/\text{H}] < -1.2$). For this group we conclude that there is no evidence of age spread. We consider the clusters NGC 5272 (M3), NGC 6205 (M13) and NGC 1904. As in previous studies, we find that M13 results formally older than M3,

with NGC 1904 between the two, but these differences are still within the observational errors, and therefore not significant. On the contrary, C96 find M13 as much as ~ 2 Gyr older than M3, but the recent accurate photometry of JB98 agrees with our and earlier results.

Intermediate metallicity group ($-1.2 \leq [\text{Fe}/\text{H}] < -0.9$). For this group we found clear evidence of age dispersion, with clusters up to $\sim 25\%$ younger than the older members of the group. We will center our attention on NGC 1851, NGC 1261, NGC 288, NGC 2808 and NGC 362. As in the present paper, NGC 2808 is found to be younger by previous investigations (C96, R96 and B98). NGC 1851 is found young by C96, B98, SW98, R96 and the present work, while S96 claim that NGC 1851, NGC 362 and NGC 288 are coeval.

NGC 288 and NGC 362 have been often compared in the past: apart from C96, all the previous investigations were based on the CMD obtained by Bolte (1987, 1989). Bolte (1989), C96, R96, V90, and SD90 claim that NGC 362 is significantly younger than NGC 288 (a $\sim 15 - 20\%$ lower age, in agreement with our result). A different interpretation of the same data is offered by B98 and SW98, who did not find significant age differences. Still, most of the past studies agree with our finding of a somewhat lower age for NGC 362 with respect to NGC 288. In the case of NGC 1261, apart from C96 (based on Ferraro 1993), past investigations were based on the CMD published by Bolte & Marleau (1989). We find that this cluster is $\sim 25\%$ younger than NGC 288, and this result goes in the same sense of C96, R96 and Bolte (1989), although the size of the age offset is different. In contrast, B98 find no age difference and SW98 find the cluster even older than NGC 288. It is difficult to identify the origin of the difference with respect to the last two investigations, since no value for the age indicators is given by SW98, and B98 use V_{05} as representative of the TO luminosity: since the Bolte & Marleau CMD becomes quite confused just below the TO level, it is possible that the B98 value is affected by a large error. On the contrary,

our CMD is better defined and more populated, allowing a more reliable definition of the fiducial branches. For comparison, our $\Delta V^{0.05}$ estimate would be 0.25 mag brighter than in B98, i.e. we would still find a younger age.

High metallicity group ($[\text{Fe}/\text{H}] \geq -0.9$). Except for the case of Pal 12, our conclusion for this group is that these clusters are coeval, within the uncertainties, and possibly younger than the lower metallicity ones. Most previous studies also determined a constant age for this group, with the only exception of C96. For NGC 104 and NGC 6838 all previous studies used the same datasets (i.e. Hesser et al. 1987 and Hodder et al. 1992 for the two clusters, respectively), while in the case of NGC 6352 the Fullton et al. (1995) CMD was used by C96 and R96, and that of Buonanno et al. (1997) was used by SW98 and B98. We can therefore take the C96 discrepant result as a sign of the inherent uncertainties of the combined photometric databases and measurement procedures. Indeed, the SW98, B98 and the present ages, which are based on two independent methods, are all in fairly good agreement.

5.3. Radial Distribution of Age

Some important clues on the Milky Way formation and early evolution can be obtained from the Galactocentric radial distribution of the GGC relative ages. It is represented in Fig. 5 (right panels) and covers the Galactic zone between 2 and 18.5 kpc. The R_{GC} values have been taken from Tab. 1.

We can clearly distinguish two groups of clusters: the old (coeval) and a smaller sample of younger clusters. The two groups are better seen in the lower panel (but see comments on the errors associated with the vertical parameter in Section 4.1).

We begin our discussion with those clusters significantly younger than the bulk. They have at least a 10% younger age. Within this group we should distinguish between the “really younger” (NGC 1261, NGC 1851, NGC 2808, NGC 362 and Pal 12), which have an older counterpart at the same metallicity which turns out to be coeval with the other most metal poor objects, and those lacking an old counterpart with similar metallicity, for which the younger age is deduced by comparison with the models, and hence is model dependent (NGC 104, NGC 6352, NGC 6366 and NGC 6838). In the last (most metal rich) group, four of the five clusters lie within 8 kpc from the Galactic center. A young age for three of them was already suggested by Salaris & Weiss (1998), who find, as we do, an almost null age difference within this group, and an average age $\sim 20\%$ younger than the metal-poor halo clusters.

Beyond 8 kpc, five younger clusters are seen in Fig. 5, namely NGC 362, NGC 2808, Pal 12, NGC 1851 and NGC 1261 (in order of increasing R_{GC}).

Coming to the bulk of our cluster sample, we already noticed that for the coeval clusters there is a small age dispersion around the mean zero level ($\sim 4\%$ for the coeval sample), which is consistent with a null dispersion when we take into account the observational errors. This dispersion is much larger if we consider the whole sample, but we do not find any Galactocentric distance vs. age relation. However, it is interesting that, if the (uncertain) metal rich clusters (marked by open diamonds in Fig. 5) were excluded, it would appear that the age spread increases with the Galactocentric radius. This result has been reached also by Richer et al. (1996), Chaboyer et al. (1996), Salaris & Weiss (1998), Buonanno et al. (1998), who include clusters out to 100 kpc, 37 kpc, 27 kpc and 28 kpc respectively. All these studies remark that younger clusters are present only in the outer regions.

In summary, as a matter of fact, the following picture arises from our analysis:

- According to the current models, most of the clusters are coeval and old.
- A fraction of the intermediate metallicity and all the metal rich clusters (according to the current models) are substantially younger.
- The younger intermediate metallicity clusters have all $R_{GC} > 8$ kpc.
- The young clusters located at larger R_{GC} have typical halo kinematics.

The consequences of these results on the mechanism of halo formation are discussed in the next section.

6. Clues on the Milky Way Formation

Fig. 7 shows how the mean normalized relative ages (Col. 7 of Table 2) compare with previous large-scale investigations: the different panels show, from top to bottom, histograms of the normalized age distributions found by Chaboyer et al. (1996), Richer et al. (1996), Salaris & Weiss (1998), Buonanno et al. (1998), and the present study. In order to intercompare them, they have been normalized to the mean absolute age in each author's scale. For each histogram, the shadowed area corresponds to GGCs with a Galactocentric distance smaller than 20 kpc.

It is clear that the age distributions become narrower as we go from older to more recent studies. This is just the sign of the increasing accuracy of the data samples, of the measurement procedures, and of the analysis techniques. The principal improvements that we have introduced are: (a) the use of the largest homogeneous CCD database (meaning with homogeneous that the same instrumentation has been used, the same data and photometric reduction procedures have been followed for all clusters, the same calibration standards have been adopted, etc...); (b) the use of two independent methods for the age

measurement; (c) the use of V , I photometry, and (d) a homogeneous metallicity scale and recent theoretical models are also introduced.

The age dating progress that has been discussed so far has important consequences on our interpretation of the timescales of the Milky Way formation. In particular, we go from a halo formation lasting for $\sim 40\%$ of the Galactic lifetime (C96), to the present result of most of the halo clusters being coeval.

Besides this basic result, other clues on the Milky Way formation have been obtained from the previous discussion. Going back to Fig. 5, a chronological order of structure formation can be inferred. The first objects to be formed are the halo clusters. Old clusters are found at any distance from the Galactic center.

The GC formation process then started at the same zero age throughout the halo, at least out to ~ 20 kpc from the center. All the more metal rich ($[\text{Fe}/\text{H}] \geq -0.9$) clusters formed at later times ($\sim 17\%$ of the halo age). Once again, we stress that this interpretation is model dependent, as it depends on the behavior of the isochrones at high metallicities, and it is based on only 5 objects. Note that these clusters do not identify a unique substructure of the Galaxy. One (Pal 12), likely two (including NGC 6366, cf. Da Costa & Armandroff (1995)) are halo members, one might be a member of the bulge population (NGC 6352, Minniti 1995), and the last two (NGC 6838 and 47 Tuc) of more uncertain classification, either thick disk members (Armandroff 1989) or halo clusters crossing the disk, following Minniti (1995) who showed that there is no thick disk GGC population.

Finally, significantly younger halo GGCs are found at any $R_{\text{GC}} > 8$ kpc. These clusters (Pal 12, NGC 1851, NGC 1261, NGC 2808 and NGC 362) could be associated with the so-called “streams”, i.e. alignments along great circles over the sky, which could arise from these clusters being the relics of ancient Milky Way satellites of the size of a dwarf galaxy (e.g. Lynden-Bell & Lynden-Bell 1995, Fusi Pecci et al. 1995).

7. Conclusions

Based on a new large, homogeneous photometric database for 34 Galactic globular clusters (+ Pal 12), a set of distance and reddening independent relative age indicators has been measured. The $\delta(V - I)_{@2.5}$ and $\Delta V_{\text{TO}}^{\text{HB}}$ vs. metallicity relations have been compared to the relations predicted by two recent updated libraries of isochrones. Using these models and two independent methods, we have found that self-consistent relative ages can be estimated for our GGCs sample. In turn, this demonstrates that the two adopted models are internally self-consistent.

Based on the relative age vs. metallicity distribution, we conclude that there is no evidence of an age spread for clusters with $[\text{Fe}/\text{H}] < -1.2$, all 19 clusters of our sample in this metallicity range being old and coeval. For the intermediate metallicity group ($-1.2 \leq [\text{Fe}/\text{H}] < -0.9$) there is a clear evidence of age dispersion, with clusters up to $\sim 25\%$ younger than the older members. Seven of the 11 GGCs in this group are coeval (also with the previous group), while the remaining 4 are much younger (namely NGC 362, NGC 1261, NGC 1851 and NGC 2808). Finally, the metal rich group ($[\text{Fe}/\text{H}] \geq -0.9$) seem to be coeval within the uncertainties (except Pal 12), and younger ($\sim 17\%$) than the rest of the clusters, this result being model dependent.

From the Galactocentric distribution of the GGC ages, we can divide the GGCs in two groups, the old coeval clusters, and the young clusters. The second group should be divided in two subgroups, the “real young clusters” and the “model dependent”, located in the intermediate and high metallicity groups, respectively. From this distribution, we can present a possible interpretation of the Milky Way formation:

- The GC formation process started at the same zero age throughout the halo, at least out to ~ 20 kpc from the Galactic center.

- At later ($\sim 17\%$ lower) times the metal-rich globulars are formed (we stress that this interpretation is model dependent).
- Finally, significantly younger halo GGCs are found at any $R_{GC} > 8kpc$, for which a possible scenario associated with mergers of dwarf galaxies to the Milky Way could be considered.

A. Theoretical model fitting

As already introduced in Sect. 3.4, and in order to interpret the results of our data samples, the theoretical isochrones computed by Straniero et al. (1997, SCL97), Cassisi et al. (1998, C98), and Vandenberg et al. (1999, V99) were used. On these isochrones, the same morphological parameters already defined for the observational CMDs (ΔV_{TO}^{HB} and $\delta(V - I)_{@2.5}$), were measured.

The trends of the theoretical quantities as a function of both age and metallicity were least-square interpolated by means of third-order polynomials, so that the observed parameters can be easily mapped into age and metallicity variations. This will allow us to easily translate the parameter values into ages.

The equations used are of the form:

$$Parameter = a + b \cdot [Fe/H] + c \cdot (\log t) + d \cdot [Fe/H]^2 + e \cdot (\log t)^2 + f \cdot [Fe/H] \cdot (\log t) + g \cdot [Fe/H]^3 + h \cdot (\log t)^3 + i \cdot [Fe/H]^2 \cdot (\log t) + j \cdot [Fe/H] \cdot (\log t)^2,$$

where *parameter* represents one of the two photometric age indices (ΔV_{TO}^{HB} or $\delta(V - I)_{@2.5}$) and t is the age in Gyr.

The $[Fe/H]$ of the V99 models were provided by the authors, while for the SCL97 and C98 models they were defined as $[Fe/H] = \log(Z/Z_{\odot})$, setting $Z_{\odot} = 0.02$. The resulting

coefficients are listed in Tab. 3, where the last line also reports the *rms* of the fits in magnitude and age.

An example of our fits can be seen in Fig. 8. The upper left panel shows the $\delta(V - I)_{@2.5}$ vs. log age theoretical behavior (at constant $[\text{Fe}/\text{H}]$), while the upper right panel shows the same parameter vs. $[\text{Fe}/\text{H}]$ (at constant ages). In both panels, model results are shown by open circles, while our fits are represented by solid lines. In the lower panels, the absolute residuals of the respective fits are presented. The maximum difference between the model and our fit is 0.006 mag, and the standard deviation ~ 0.0015 mag, which correspond to 0.15 Gyr. The dotted lines graphically represent these two values.

A second order polynomial would not be able to follow the theoretical trend of the models, while the distribution of the residuals shows that a fourth order is not required, since the residual uncertainty is much smaller than the observational error.

B. A test bench for the theoretical models

One can look at Fig. 3 and 4 as empirical calibrations of the two differential parameters $\Delta V_{\text{TO}}^{HB}$ and $\delta(V - I)_{@2.5}$ as a function of $[\text{Fe}/\text{H}]$. Assuming that the two differential parameters are controlled just by the age and the metallicity, when the theoretical loci are superposed to these two diagrams, the same age-metallicity relations must be obtained in the two cases.

We have shown that this is true for the the Straniero et al. (1997, SCL97) and VandenBerg et al. (1999, V99) models, which indeed yield the same (shallow) age-metallicity relation both using $\Delta V_{\text{TO}}^{HB}$ and $\delta(V - I)_{@2.5}$.

The same is not true for the C98 models: looking at Fig. 9 it is clear that the theoretical isochrones show the same trend seen for the other two sets of models in the lower panel

(vertical method), while, for example, an age-metallicity relation of $\sim +5$ Gyr/dex for $[\text{Fe}/\text{H}] < -1$ appears when the horizontal parameter is used (inconsistent with the upper panel, and with what we have using SCL97 and V99 models). In order to reconcile the two diagrams, one could play with the HB luminosity-metallicity relation. After a few tests, we found that a partial agreement could be reached by using $M_V(\text{HB}) = 0.35 [\text{Fe}/\text{H}] + 1.40$, but such faint values for the RR Lyr luminosity are not consistent with the most recent results (see e.g. Carretta et al. 1999), and the age-metallicity relation would disagree in any case at the high $[\text{Fe}/\text{H}]$ end.

We also checked the $B - V$ behavior of the horizontal parameter for the C98 models, and in that case they agree with the SCL97 ones.

It is therefore suggested that the problems in the C98 isochrones is related to the I bolometric corrections (which indeed are different from those used by both SCL97 and V99).

This test shows how our database can be used to define useful observational constraints that any model calculation must reproduce. Furthermore, we also suggest that a *multicolor* approach should be followed to fully test the theoretical models.

We thank Santino Cassisi and Alessandro Chieffi for providing us with their models in tabular form. We are indebted to Don Vandenberg for sending us his isochrones in advance of publication. We thank Vittorio Castellani, Sergio Ortolani, Peter Stetson, and Don Vandenberg for the useful discussions and encouragements. GP, IS, and AR acknowledge partial support by the Ministero della Ricerca Scientifica e Tecnologica and by the Agenzia Spaziale Italiana. AR has been supported by the Italian Consorzio Nazionale Astronomia e Astrofisica.

REFERENCES

- Armandroff T.E., 1989, AJ, 97, 375
- Bertelli G., Bressan A., Chiosi C., Fagotto F., Nasi E., 1994, A&AS, 106, 275
- Bolte M., 1987, ApJ, 315, 469
- Bolte M., 1989, AJ, 97, 1688
- Bolte M., Marleau F., 1989, PASP, 101, 1088
- Buonanno R., Corsi C.E., Pulone L., Fusi Pecci F., Bellazzini M., 1998, A&A, 333, 505
- Buonanno R., et al., 1997, (in preparation)
- Carretta E., Gratton R., 1997, A&AS, 121, 95
- Carretta E., Gratton R., Clementini G., Fusi Pecci F., 1999, astro-ph/9902086
- Cassisi S., Castellani V., Degl’Innocenti S., Weiss A., 1998, A&AS, 129, 267 (C98)
- Chaboyer B., Demarque P., Sarajedini A., 1996, ApJ, 459, 558 (C96)
- Da Costa G.S., Armandroff T.E., 1995, AJ, 109, 2533
- Ferraro F.R., Clementini G., Fusi Pecci F., Vitiello E., Buonanno R., 1993, MNRAS, 264,
273
- Fullton L.K. et al., 1995, AJ, 110, 652
- Fusi Pecci F., Bellazzini M., Cacciari C., Ferraro F.R., 1995, AJ, 110, 1664
- Gratton R.G., Ortolani S., 1988, A&AS, 73, 137
- Harris W.E., 1996, AJ, 112, 1487

- Hesser J.E., Harris W.E., Vandenberg D.A., Allwright J.W.B., Shott P., Stetson P.B., 1987, PASP, 99, 739
- Hodder P.J.C., Nemec J.M., Richer H.B., Fahlman G.G., 1992, AJ, 103, 460
- Johnson J.A., Bolte M., 1998, AJ, 115, 693 (JB98)
- Landolt A.U. 1992, AJ 104, 340
- Lynden-Bell D., Lynden-Bell R. M., 1995, MNRAS, 275, 429
- Minniti D., 1995, AJ, 109, 1663.
- Richer H.B. et al., 1996, ApJ, 463, 602 (R96)
- Rosenberg A., Saviane I., Piotto G., Aparicio A., Zaggia S. R., 1998a, AJ, 115, 648
- Rosenberg A., Saviane I., Piotto G., Held E. V., 1998b, A&A, 339, 61 (PAPER III)
- Rosenberg A., Piotto G., Saviane I., Aparicio A., 1999a, A&AS, submitted (PAPER I)
- Rosenberg A., Aparicio A., Saviane I., Piotto G., 1999b, A&AS, submitted (PAPER II)
- Rutledge A.G., Hesser J.E., Stetson P.B., 1997, PASP, 109, 907
- Salaris M., Weiss A., 1998, A&A, 335, 943 (SW98)
- Sandquist E.L., Bolte M., Langer G.E., Hesser J.E., Mendes de Oliveira C., 1999, ApJ, 518, 262
- Sarajedini A., Chaboyer B., Demarque P., 1997, PASP, 109, 1321
- Sarajedini A., Demarque P., 1990, ApJ, 365, 219 (SD90)
- Saviane I., Rosenberg A., Piotto G., 1997. In: R.T. Rood & A.Renzini (eds.) Advances in Stellar Evolution, Cambridge University Press, Cambridge, p. 65 (SRP97)

- Saviane I., Rosenberg A., Piotto G., 1999. In: B.K. Gibson, T.S. Axelrod & M. E. Putman (eds.), ASP Conference Series, in press
- Saviane I., Rosenberg A., Piotto G., Aparicio A., 1999, A&A, submitted.
- Stetson P.B., Vandenberg D.A., Bolte M., 1996, PASP, 108, 560 (S96)
- Stetson P.B., Vandenberg D.A., Bolte M., Hesser J.E., Smith G.H., 1988, AJ 97, 1360
- Straniero O., Chieffi A., Limongi M., 1997, ApJ, 490, 425 (SCL97)
- Sweigart A.V., 1997, ApJ, 474, 23
- Vandenberg D.A., Swenson F.J., Rogers F.J., Iglesias C.A., Alexander D.R., 1999, ApJ, submitted (V99)
- Vandenberg D.A., Bolte M., Stetson P.B., 1990, AJ, 100, 445 (V90)
- Vandenberg D.A., Stetson P.B., Bolte M. 1996, ARA&A, 34, 461
- Zinn R., West M., 1984, ApJS, 55, 45

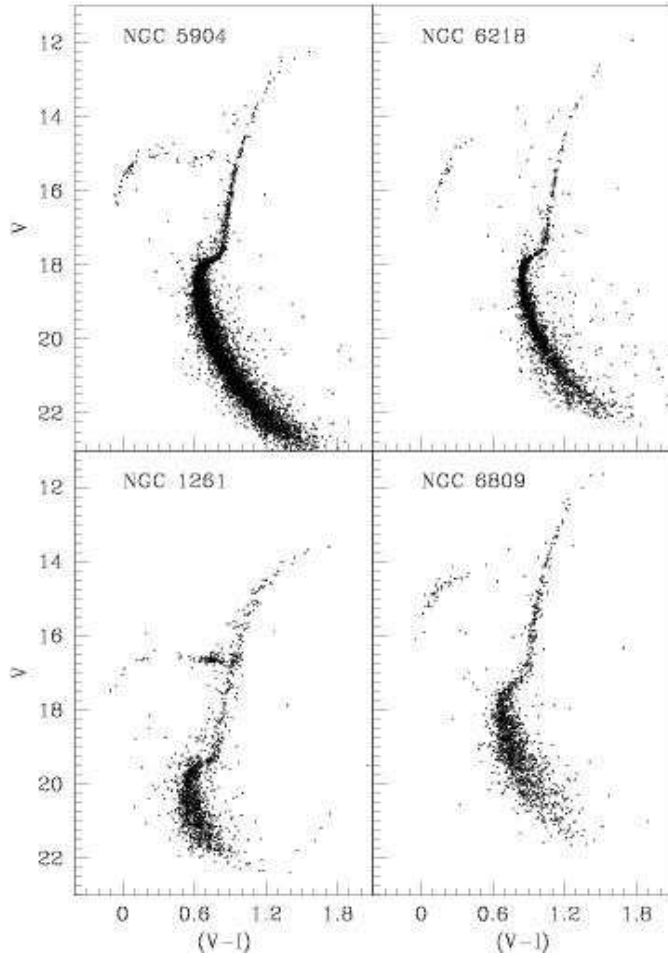


Fig. 1.— The CMDs of 4 clusters used in the relative age determination, which show the range in quality that is spanned by the present data set. The top panels show two of the best CMDs (for the clusters NGC 5904 and NGC 6218); NGC 6809 and NGC 1261 (lower panels) are an example of lower quality photometric samples. In each case, the HB is populated by a good number of stars, and more than 1 mag below the TO is covered even in the case of NGC 1261.

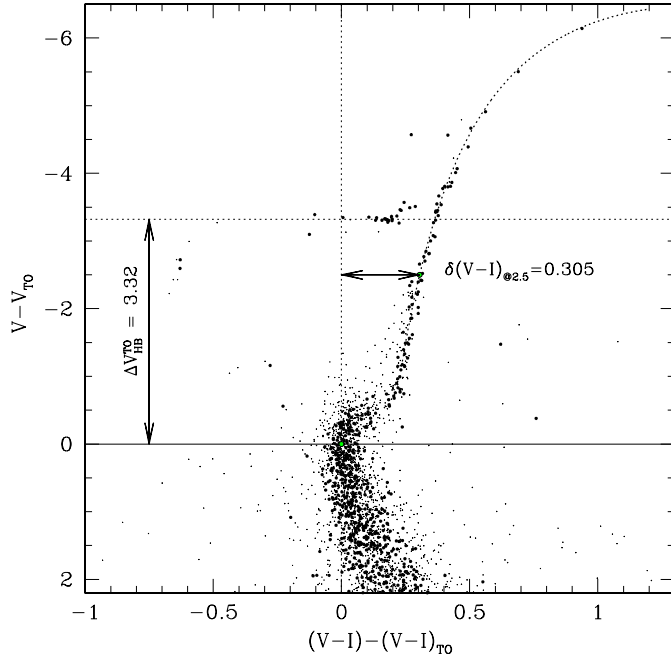


Fig. 2.— The CMD of NGC 1851. The heaviest points represent the selected CMD used to measure the TO position and to fit the RGB fiducial line. Magnitude and color have been registered to the TO point. The vertical $\Delta V_{\text{TO}}^{\text{HB}}$ and horizontal $\delta(V-I)_{@2.5}$ parameter values for this cluster are indicated by arrows. The analytical fit to the RGB is also shown.

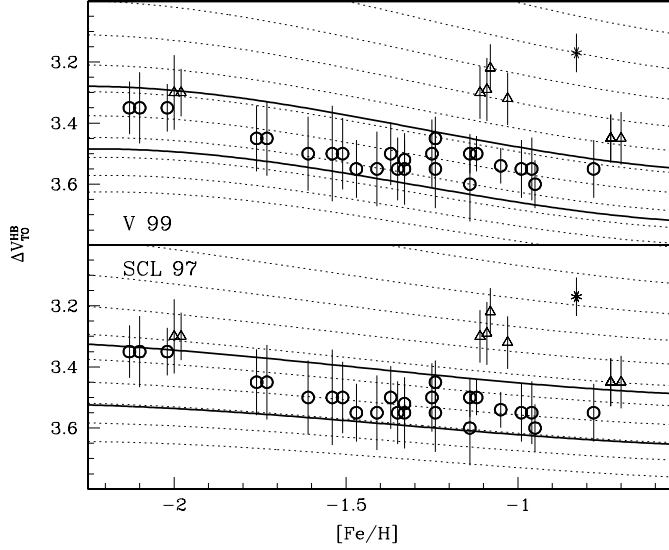


Fig. 3.— The measured ΔV_{TO}^{HB} parameter is plotted versus the metallicity. The dotted lines in the two panels show the theoretical trend for V99 (*top*) and SCL97 (*bottom*) models. The isochrones are spaced by 1 Gyr (starting from 18 Gyr at the bottom). The asterisk represents the cluster Pal 12. The two isochrones displayed as solid lines represent the ± 1 standard deviation limits of the ΔV_{TO}^{HB} parameter for the entire sample (excluding Pal 12), and clusters falling within these (circles), are defined as “fiducial coeval”. Note that the two independent models give the same fiducial coeval object selection.

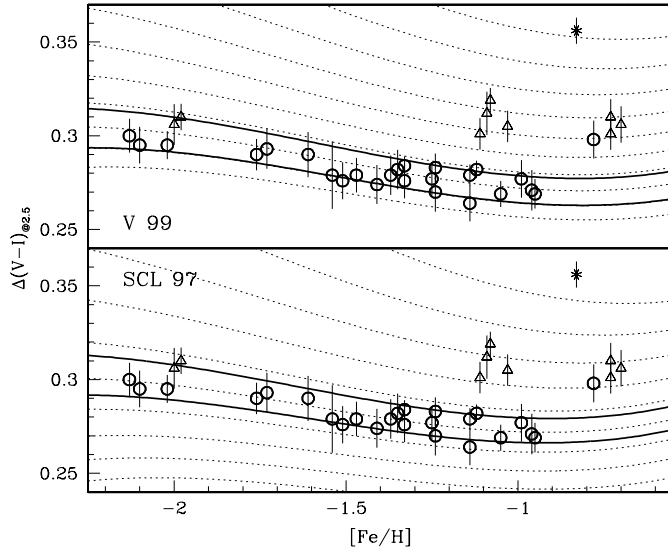


Fig. 4.— The measured $\delta(V - I)_{@2.5}$ parameter is plotted versus metallicity. The same two sets of theoretical models of Fig. 3 are shown (dotted lines). Age is spaced in 1 Gyr steps, the lowermost line corresponding to 18 Gyr and 17 Gyr isochrones, for V99 and SCL97, respectively. The fiducial coeval clusters selected in Fig. 3 are plotted as *open circles*. The two isochrones displayed as solid lines represent the ± 1 standard deviation limits of the $\delta(V - I)_{@2.5}$ parameter for the GGC sample (except Pal 12). Notice that the two clusters at $[\text{Fe}/\text{H}] = -0.73$ (NGC 6366 and NGC 6838) have the same $\Delta V_{\text{TO}}^{\text{HB}}$, so they appear as a single point in Fig. 3.

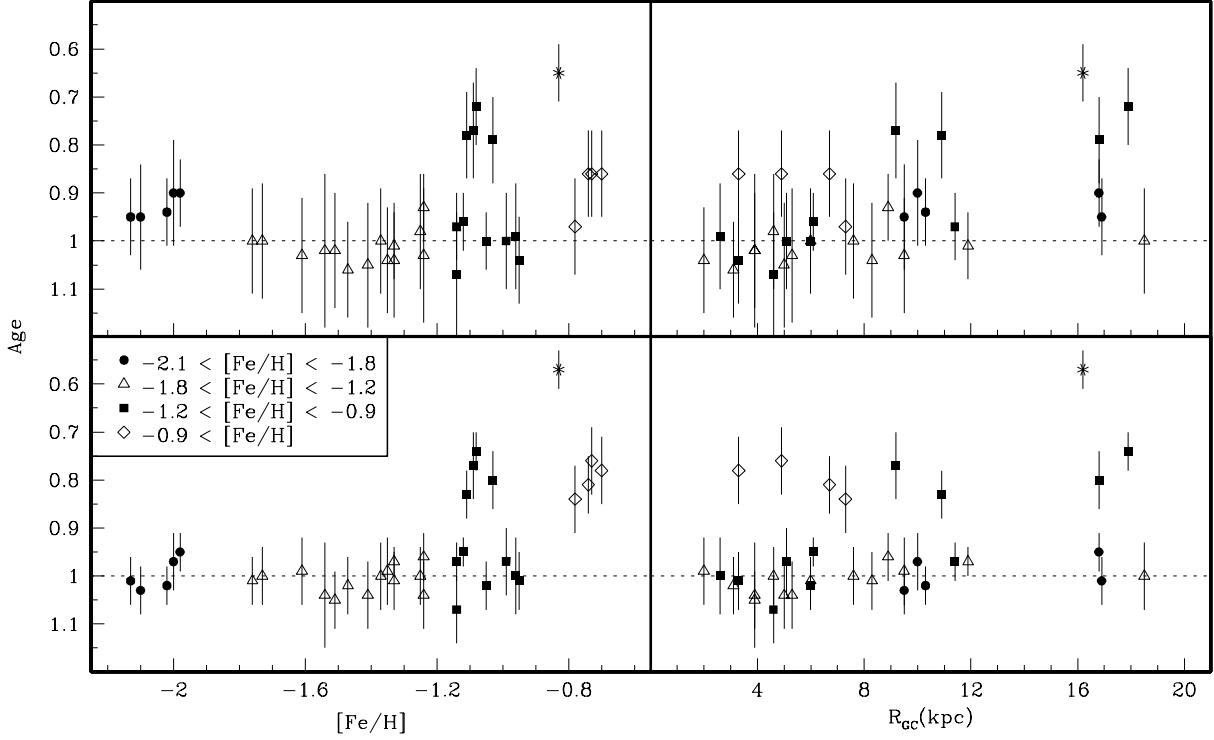


Fig. 5.— The normalized relative ages for our Gc sample from the vertical (top panels) and the horizontal (bottom panels) methods are plotted versus the metallicity (*left panels*) and versus the Galactocentric distance (*right panels*). The different symbols represent clusters in different metallicity groups as indicated in the lower left panel. The error bars are the mean errors as given in cols. 3 and 5 of Tab. 2. The youngest cluster (marked by an asterisk) is Pal 12.

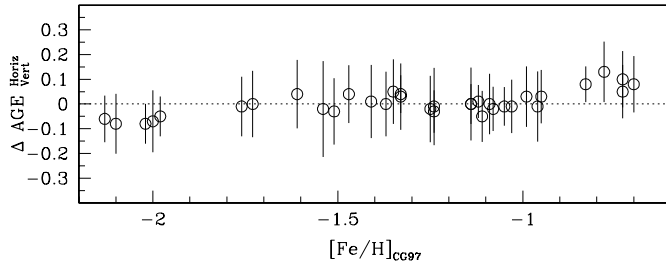


Fig. 6.— The difference in the normalized relative ages obtained from the two methods, $\Delta \text{Age}_{\text{Vert}}^{\text{Horiz}}$, as a function of the metallicity. The error bars were obtained as the quadratic sum of the errors from the two methods.

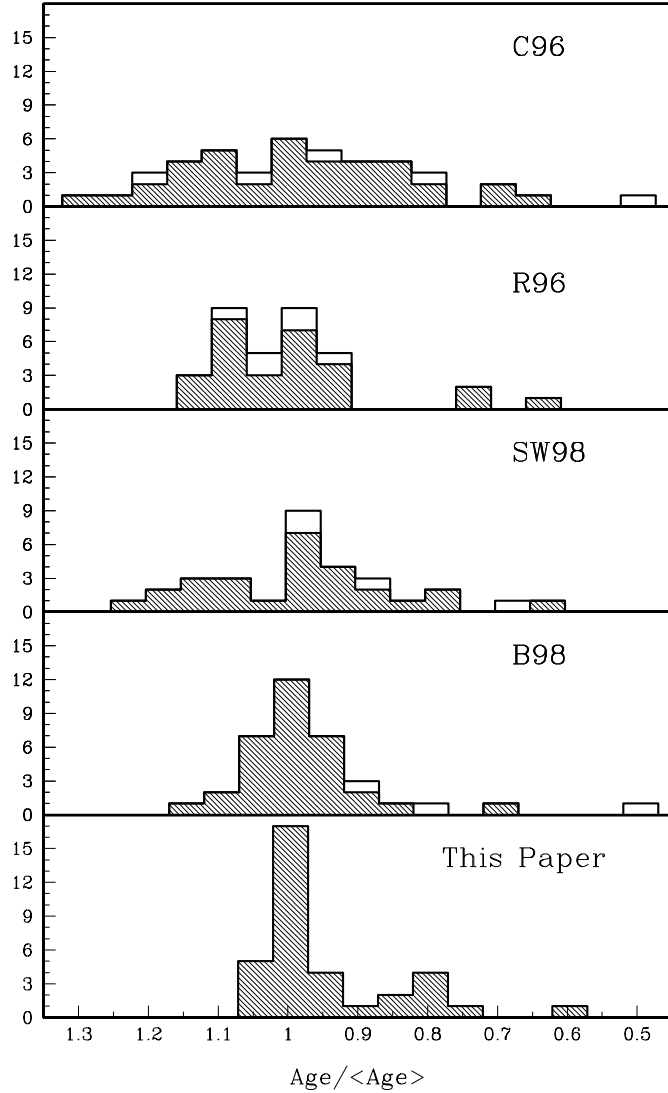


Fig. 7.— Histograms of the relative age distribution from the most recent compilations in the literature. The histograms are centered on the mean age of the respective samples. Clusters located at the right are younger. The shadowed zone represent the histogram for clusters within 20 kpc from the center of our Galaxy. The labels identify previous investigations, as explained in the text.

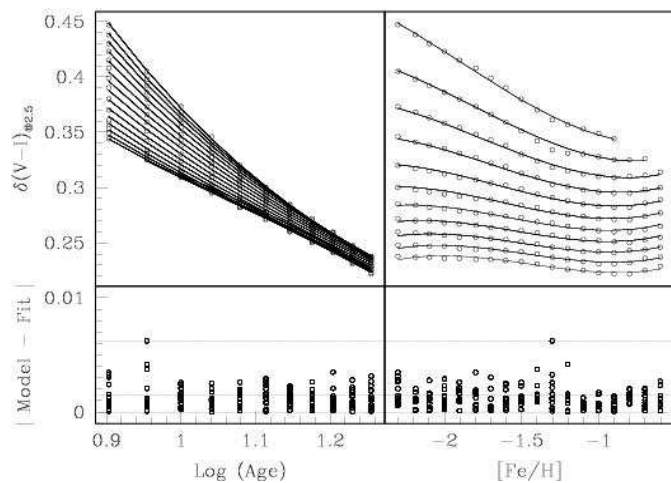


Fig. 8.— Example of our fit to the SCL97 models. The measured values on the theoretical models are fitted in both the $\delta(V - I)_{@2.5}$ vs $[\text{Fe}/\text{H}]$ plane (upper-right panel) and the $\delta(V - I)_{@2.5}$ vs. $\log t$ plane (upper-left panel). The fit to the theoretical values (open circles) are shown as continuous lines. The bottom panels show the residuals

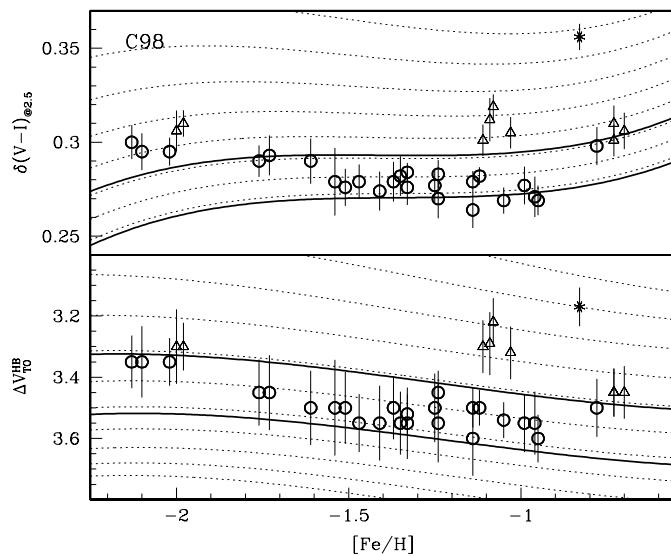


Fig. 9.— The same as in Figs. 3 and 4, but for the models of C98.

Table 1. Data for the 34 (+Pal 12) analyzed GGCs.

In the following cases, the [Fe/H] values were taken from: ^(a) CG97 and ^(b) ZW84 (transformed to the CG97 scale, as given by CG97).

	Cluster	[Fe/H]	R_{GC}	$V(TO)$	$(V - I)_{(TO)}$	$V(HB)$	ΔV_{TO}^{HB}	$\delta(V - I)_{@2.5}$
01	NGC 104	-0.78 ± 0.02	7.3	17.60 ± 0.08	0.660 ± 0.007	14.05 ± 0.05	3.55 ± 0.09	0.295 ± 0.010
02	NGC 288	-1.14 ± 0.03	11.4	18.90 ± 0.04	0.645 ± 0.002	15.40 ± 0.05	3.55 ± 0.06	0.276 ± 0.006
03	NGC 362	-1.09 ± 0.03	9.2	00.00 ± 0.09	0.000 ± 0.008	03.29 ± 0.05	3.29 ± 0.10	0.312 ± 0.011
04	NGC 1261	-1.08 ± 0.04	17.9	19.90 ± 0.06	0.555 ± 0.003	16.68 ± 0.05	3.22 ± 0.08	0.319 ± 0.007
05	NGC 1851	-1.03 ± 0.06	16.8	19.50 ± 0.07	0.630 ± 0.005	16.18 ± 0.05	3.32 ± 0.09	0.305 ± 0.008
06	NGC 1904	-1.37 ± 0.05	18.5	19.65 ± 0.09	0.610 ± 0.007	16.15 ± 0.05	3.50 ± 0.10	0.279 ± 0.010
07	NGC 2808	-1.11 ± 0.03	10.9	19.60 ± 0.07	0.800 ± 0.005	16.30 ± 0.05	3.30 ± 0.09	0.301 ± 0.008
08	NGC 3201	-1.24 ± 0.03	8.9	18.20 ± 0.05	0.905 ± 0.004	14.75 ± 0.05	3.45 ± 0.07	0.283 ± 0.008
09	NGC 4590	-2.00 ± 0.03	10.0	19.05 ± 0.07	0.605 ± 0.006	15.75 ± 0.10	3.30 ± 0.12	0.306 ± 0.010
10	NGC 5053	-1.98 ± 0.09	16.8	20.00 ± 0.06	0.545 ± 0.004	16.70 ± 0.05	3.30 ± 0.08	0.310 ± 0.007
11	NGC 5272	-1.33 ± 0.02^a	11.9	19.10 ± 0.04	0.575 ± 0.002	15.58 ± 0.05	3.52 ± 0.06	0.284 ± 0.005
12	NGC 5466	-2.13 ± 0.36^b	16.9	19.95 ± 0.07	0.555 ± 0.006	16.60 ± 0.05	3.35 ± 0.09	0.300 ± 0.009
13	NGC 5897	-1.73 ± 0.07	7.6	19.75 ± 0.07	0.720 ± 0.006	16.30 ± 0.10	3.45 ± 0.12	0.293 ± 0.011
14	NGC 5904	-1.12 ± 0.03	6.1	18.50 ± 0.03	0.625 ± 0.002	15.00 ± 0.05	3.50 ± 0.06	0.282 ± 0.005
15	NGC 6093	-1.47 ± 0.04	3.1	19.80 ± 0.08	0.815 ± 0.005	16.25 ± 0.05	3.55 ± 0.09	0.279 ± 0.009
16	NGC 6121	-1.05 ± 0.03	6.0	16.90 ± 0.03	1.125 ± 0.004	13.36 ± 0.05	3.54 ± 0.06	0.269 ± 0.007
17	NGC 6171	-0.95 ± 0.04	3.3	19.25 ± 0.06	1.150 ± 0.004	15.65 ± 0.05	3.60 ± 0.08	0.269 ± 0.007
18	NGC 6205	-1.33 ± 0.05	8.3	18.50 ± 0.06	0.575 ± 0.004	14.95 ± 0.10	3.55 ± 0.12	0.276 ± 0.009
19	NGC 6218	-1.14 ± 0.05	4.6	18.30 ± 0.07	0.850 ± 0.004	14.70 ± 0.10	3.60 ± 0.12	0.264 ± 0.010
20	NGC 6254	-1.25 ± 0.03	4.6	18.55 ± 0.05	0.930 ± 0.003	15.05 ± 0.10	3.50 ± 0.11	0.277 ± 0.009
21	NGC 6341	-2.10 ± 0.02^a	9.5	18.55 ± 0.06	0.555 ± 0.005	15.20 ± 0.10	3.35 ± 0.12	0.295 ± 0.010
22	NGC 6352	-0.70 ± 0.02	3.3	18.70 ± 0.07	0.985 ± 0.007	15.25 ± 0.05	3.45 ± 0.09	0.306 ± 0.010
23	NGC 6362	-0.99 ± 0.03	5.1	18.90 ± 0.08	0.685 ± 0.007	15.35 ± 0.05	3.55 ± 0.09	0.277 ± 0.010
24	NGC 6366	-0.73 ± 0.05	4.9	19.10 ± 0.06	1.570 ± 0.005	15.65 ± 0.05	3.45 ± 0.08	0.310 ± 0.009
25	NGC 6397	-1.76 ± 0.03	6.0	16.40 ± 0.04	0.775 ± 0.002	12.95 ± 0.10	3.45 ± 0.11	0.290 ± 0.008
26	NGC 6535	-1.51 ± 0.10	3.9	19.30 ± 0.06	1.105 ± 0.004	15.80 ± 0.10	3.50 ± 0.12	0.270 ± 0.010
27	NGC 6656	-1.41 ± 0.03^a	5.0	17.80 ± 0.07	0.960 ± 0.005	14.25 ± 0.10	3.55 ± 0.12	0.274 ± 0.010
28	NGC 6681	-1.35 ± 0.03	2.0	19.25 ± 0.09	0.690 ± 0.007	15.70 ± 0.05	3.55 ± 0.10	0.282 ± 0.011
29	NGC 6723	-0.96 ± 0.04	2.6	19.00 ± 0.09	0.725 ± 0.007	15.45 ± 0.05	3.55 ± 0.10	0.271 ± 0.011
30	NGC 6752	-1.24 ± 0.03	5.3	17.35 ± 0.08	0.705 ± 0.005	13.80 ± 0.10	3.55 ± 0.13	0.270 ± 0.010
31	NGC 6779	-1.61 ± 0.13^b	9.5	19.80 ± 0.11	0.840 ± 0.008	16.30 ± 0.05	3.50 ± 0.12	0.290 ± 0.012
32	NGC 6809	-1.54 ± 0.03	3.9	17.95 ± 0.12	0.680 ± 0.014	14.45 ± 0.10	3.50 ± 0.16	0.279 ± 0.018
33	NGC 6838	-0.73 ± 0.03	6.7	17.95 ± 0.06	0.935 ± 0.005	14.50 ± 0.05	3.45 ± 0.08	0.301 ± 0.008
34	NGC 7078	-2.02 ± 0.04	10.3	19.25 ± 0.06	0.650 ± 0.004	15.90 ± 0.05	3.35 ± 0.08	0.295 ± 0.007
35	Pal 12	-0.83 ± 0.06	16.2	20.35 ± 0.06	0.695 ± 0.005	17.18 ± 0.02	3.17 ± 0.06	0.356 ± 0.007

Table 2. Galactic globular clusters relative ages. The last column indicates if the cluster is coeval (C), younger (Y) or probably younger(Y?).

Cluster name		Vertical Method		Horizontal Method		Mean Age		
NGC	Other	\overline{Age}	$\Delta Age(Gyr)$	\overline{Age}	$\Delta Age(Gyr)$	\overline{Age}	$\Delta Age(Gyr)$	
104	47 Tucanae	0.97 ± 0.10	-0.4 ± 1.4	0.84 ± 0.07	-2.0 ± 0.9	0.90 ± 0.08	-1.2 ± 1.2	Y?
288	-	0.97 ± 0.07	-0.3 ± 0.9	0.97 ± 0.04	-0.3 ± 0.5	0.97 ± 0.05	-0.3 ± 0.7	C
362	-	0.77 ± 0.10	-2.9 ± 1.4	0.77 ± 0.07	-2.9 ± 1.0	0.77 ± 0.08	-2.9 ± 1.2	Y
1261	-	0.72 ± 0.08	-3.6 ± 1.0	0.74 ± 0.04	-3.3 ± 0.5	0.73 ± 0.05	-3.5 ± 0.8	Y
1851	-	0.79 ± 0.09	-2.7 ± 1.2	0.80 ± 0.06	-2.5 ± 0.7	0.80 ± 0.07	-2.6 ± 0.9	Y
1904	M 79	1.00 ± 0.11	0.0 ± 1.4	1.00 ± 0.07	0.0 ± 0.9	1.00 ± 0.08	0.0 ± 1.2	C
2808	-	0.78 ± 0.09	-2.8 ± 1.2	0.83 ± 0.05	-2.1 ± 0.7	0.81 ± 0.07	-2.5 ± 0.9	Y
3201	-	0.93 ± 0.07	-0.8 ± 1.0	0.96 ± 0.05	-0.4 ± 0.7	0.95 ± 0.06	-0.6 ± 0.8	C
4590	M 68	0.90 ± 0.11	-1.2 ± 1.5	0.97 ± 0.06	-0.3 ± 0.7	0.94 ± 0.08	-0.8 ± 1.1	C
5053	-	0.90 ± 0.07	-1.2 ± 1.0	0.95 ± 0.04	-0.6 ± 0.5	0.93 ± 0.05	-0.9 ± 0.7	C
5272	M 3	1.01 ± 0.07	0.1 ± 0.9	0.97 ± 0.03	-0.3 ± 0.4	0.99 ± 0.05	0.0 ± 0.7	C
5466	-	0.95 ± 0.08	-0.6 ± 1.1	1.01 ± 0.05	0.1 ± 0.6	0.98 ± 0.06	-0.2 ± 0.8	C
5897	-	1.00 ± 0.12	0.0 ± 1.6	1.00 ± 0.06	0.0 ± 0.8	1.00 ± 0.09	0.0 ± 1.2	C
5904	M 5	0.96 ± 0.06	-0.4 ± 0.8	0.95 ± 0.03	-0.6 ± 0.4	0.96 ± 0.04	-0.5 ± 0.6	C
6093	M 80	1.06 ± 0.10	0.8 ± 1.3	1.02 ± 0.06	0.3 ± 0.8	1.04 ± 0.07	0.5 ± 1.0	C
6121	M 4	1.01 ± 0.06	0.0 ± 0.8	1.02 ± 0.05	0.3 ± 0.7	1.01 ± 0.05	0.1 ± 0.7	C
6171	M 107	1.04 ± 0.09	0.5 ± 1.1	1.01 ± 0.06	0.1 ± 0.8	1.02 ± 0.07	0.3 ± 0.9	C
6205	M 13	1.04 ± 0.12	0.5 ± 1.6	1.01 ± 0.06	0.1 ± 0.8	1.02 ± 0.09	0.3 ± 1.2	C
6218	M 12	1.07 ± 0.13	0.9 ± 1.7	1.07 ± 0.07	0.9 ± 0.9	1.07 ± 0.10	0.9 ± 1.3	C
6254	M 10	0.98 ± 0.12	-0.2 ± 1.5	1.00 ± 0.06	0.0 ± 0.8	0.99 ± 0.08	0.0 ± 1.2	C
6341	M 92	0.95 ± 0.11	-0.6 ± 1.4	1.03 ± 0.05	0.4 ± 0.7	0.99 ± 0.08	0.0 ± 1.1	C
6352	-	0.86 ± 0.09	-1.7 ± 1.2	0.78 ± 0.07	-2.8 ± 0.9	0.82 ± 0.08	-2.3 ± 1.1	Y?
6362	-	1.00 ± 0.10	0.0 ± 1.4	0.97 ± 0.07	-0.3 ± 0.9	0.99 ± 0.08	-0.1 ± 1.1	C
6366	-	0.86 ± 0.09	-1.7 ± 1.1	0.76 ± 0.07	-3.1 ± 0.9	0.81 ± 0.07	-2.4 ± 1.0	Y?
6397	-	1.00 ± 0.11	0.0 ± 1.4	1.01 ± 0.05	0.1 ± 0.6	1.00 ± 0.07	0.1 ± 1.0	C
6535	-	1.02 ± 0.12	0.3 ± 1.6	1.05 ± 0.06	0.7 ± 0.8	1.03 ± 0.09	0.5 ± 1.2	C
6656	M 22	1.05 ± 0.13	0.7 ± 1.7	1.04 ± 0.07	0.5 ± 0.9	1.04 ± 0.09	0.6 ± 1.3	C
6681	M 70	1.04 ± 0.11	0.5 ± 1.4	0.99 ± 0.07	0.0 ± 0.9	1.01 ± 0.08	0.2 ± 1.2	C
6723	-	0.99 ± 0.11	0.0 ± 1.5	1.00 ± 0.09	0.0 ± 1.0	1.00 ± 0.09	0.0 ± 1.3	C
6752	-	1.03 ± 0.14	0.4 ± 1.8	1.04 ± 0.07	0.5 ± 1.0	1.03 ± 0.10	0.5 ± 1.4	C
6779	M 56	1.03 ± 0.12	0.4 ± 1.6	0.99 ± 0.07	0.0 ± 1.0	1.01 ± 0.09	0.1 ± 1.3	C
6809	M 55	1.02 ± 0.16	0.3 ± 2.1	1.04 ± 0.11	0.4 ± 1.5	1.03 ± 0.13	0.4 ± 1.8	C
6838	M 71	0.86 ± 0.09	-1.7 ± 1.1	0.81 ± 0.06	-2.4 ± 0.8	0.84 ± 0.07	-2.1 ± 1.0	Y?
7078	M 15	0.94 ± 0.07	-0.7 ± 1.0	1.02 ± 0.04	0.3 ± 0.5	0.98 ± 0.05	-0.2 ± 0.8	C
-	Pal 12	0.65 ± 0.06	-4.5 ± 0.8	0.57 ± 0.04	-5.6 ± 0.6	0.61 ± 0.05	-5.0 ± 0.7	Y

Table 3. Coefficients of the polynomials used to interpolate the theoretical quantities listed as column headers.

Coeff	V99		SCL97		C98	
	$M_V(\text{TO})$	$\delta(V - I)_{@2.5}$	$M_V(\text{TO})$	$\delta(V - I)_{@2.5}$	$M_V(\text{TO})$	$\delta(V - I)_{@2.5}$
a	1.599700	0.828002	-1.580420	0.930417	11.99130	0.667046
b	0.825196	-0.165156	1.111200	-0.356030	2.550110	-0.217992
c	3.801050	-0.812187	12.85960	-1.472910	-23.50860	-0.123297
d	-0.278009	0.191788	-0.226336	0.186956	-0.331870	0.243417
e	-1.428870	0.589075	-10.29670	1.491670	21.91010	-0.008126
f	-1.153670	0.611913	-1.716990	0.970103	-4.612900	0.857613
g	-0.074459	0.021023	-0.025408	0.020722	-0.061030	0.034687
h	0.339905	-0.223764	3.240170	-0.590396	-6.108660	-0.069297
i	-0.007749	-0.077650	0.103320	-0.077396	0.094752	-0.080693
j	0.390382	-0.312448	0.754886	-0.477246	2.124730	-0.421044
<i>rms</i> :	0.017 mag (=0.23 Gyrs)	0.002 mag (=0.15 Gyrs)	0.010 mag (=0.12 Gyrs)	0.001 mag (=0.15 Gyrs)	0.017 mag (=0.20 Gyrs)	0.001 mag (=0.12 Gyrs)